JOURNAL OF MATERIALS SCIENCE **39** (2004) 7245–7251

Modelling induction skull melting design modifications

V. BOJAREVICS, K. PERICLEOUS
University of Greenwich, School of Computing and Mathematics, Park Row, London SE10 9LS, UK
E-mail: V.Bojarevics@gre.ac.uk

Induction Skull Melting (ISM) is used for heating, melting, mixing and, possibly, evaporating reactive liquid metals at high temperatures when a minimum contact at solid walls is required. The numerical model presented here involves the complete time dependent process analysis based on the coupled electromagnetic, temperature and turbulent velocity fields during the melting and liquid shape changes. The simulation is validated against measurements of liquid metal height, temperature and heat losses in a commercial size ISM furnace. The often observed limiting temperature plateau for ever increasing electrical power input is explained by the turbulent convective heat losses. Various methods to increase the superheat within the liquid melt, the process energy efficiency and stability are proposed.

1. Introduction

The Induction Skull Melting (ISM) or Cold Crucible technique is a process suitable for melting and preparing reactive metal alloys of high purity prior to casting (for the recent results see [1, 2]) or gas atomization. This process is used to melt Ti, TiAl, Zr, Mo and many other high melting temperature alloys to produce near-net-shape cast components. The technique is ideal for the treatment of reactive high temperature materials, novel composition alloys and for material property investigations [3].

An essential part of the ISM furnace is a water-cooled copper crucible used to contain the metal charge. The charge is melted by Joule heating from the induced current generated by an external medium/high frequency AC coil. The copper wall is made of electrically insulated segments so that the magnetic field can effectively penetrate through it, this penetration achieved due to high density AC current loops induced within each individual segment. These crucible currents incur relatively high energy losses with heat directly removed by the cooling liquid circulating within the copper segments. In addition to these direct Joule losses, there are other, conductive and convective heat losses from the metal charge when in contact with the crucible walls. In the case of titanium alloys, temperatures in excess of 1500°C are necessary to melt the metal and produce sufficient superheat for casting applications (for instance, near-net-shape turbine blades). The molten metal is normally held away from the side walls by the induced electromagnetic force. This critical feature affects the efficiency of the process. Contact with the wall is undesirable because it produces a thermal path from the metal to the cooling water, and also can lead to an electrical "short-circuiting" of the crucible segments. The shape and position of the liquid metal depends on the instantaneous balance of forces acting on it. Hence, the electromagnetic field and the associated force field are strongly coupled to the free surface dynamics of the liquid metal, the turbulent fluid flow within it and the heat transfer.

This complex problem has been studied extensively both experimentally [1, 2, 4, 5] and numerically [5–10]. The early numerical simulation efforts mostly concentrated on the electrodynamics part of the problem [6–8] with the heat transfer mostly treated as a stationary problem. The liquid metal shape was obtained from a magnetostatic approximation, and the turbulence of the melt velocity field was considered within the stationary k-ε type model range [8, 10]. The present model was built around the concept of a multi-physics common modelling environment [11]. The first step in the ISM model development was a semi-levitation melting numerical model [12] where the coupling between the electromagnetics and the change of the melt free surface was realised concurrently to the melting front progression. An appropriate turbulence model for the developing flow field [13] was implemented, and validated against detailed turbulent flow measurements within a 'cold' liquid metal (In-Ga-Sn) AC-field-driven experiment [14]. The numerical framework described in this paper is a successor of this first model. It features a combination of a number of complementary sub-models necessary to handle the overall complexity of the problem: finite volume, integral equation and pseudo-spectral methods are combined to achieve an accurate description of the dynamic melting process. Results presented here show the temperature history of the melting process in comparison to the experiments [4] and by account of computed heat losses in the

various parts of the equipment. Visual observations of the free surface were also compared to the numerically predicted surface shapes [15]. With the aid of detailed flow and temperature fields, numerical simulations provide explanations for the thermal efficiency loss at various stages of melting and the limitation of the resulting superheat of the melt. The experimental work used for validation was done by the University of Birmingham IRC for Materials in a collaborative project [4, 15].

The Birmingham ISM furnace uses a 7 kHz AC power supply with a 350 kW maximum power at source. At different melting stages the power is varied manually according to the process requirements to achieve a stable and reliable melt of any given material. The numerical model is used as a versatile tool to test process variations and to optimize the process for maximum superheat, stability of the melt confinement, and to indicate energy saving routines. This paper will discuss just some of the very large number of simulated process variations, reporting on results which have not been presented elsewhere. The model in addition provides the possibility for examining what-if scenarios that are not possible to test immediately on the experimental rig, which is limited by the available power supply and crucible design. So it has been possible to examine a whole range of load parameters, AC current frequency changes, and the possible application of an additional DC electromagnetic field.

2. Short description of the numerical models used

The modelling approach is based on the solution of the time dependent Reynolds-Averaged-Navier-Stokes and continuity equations for an incompressible fluid, and the heat transfer equations for the fluid and solid zones of the metal charge:

$$\partial_t \mathbf{v} + (\mathbf{v}\cdot\nabla)\mathbf{v} = -\rho^{-1}\nabla p + \nabla\cdot(\nu_e(\nabla\mathbf{v} + \nabla\mathbf{v}^T)) + \rho^{-1}\langle\mathbf{f}\rangle + \mathbf{g}, \quad (1)$$

$$\nabla\cdot\mathbf{v} = 0, \quad (2)$$

$$C_p^*(\partial_t T + \mathbf{v}\cdot\nabla T) = \nabla\cdot(C_p\alpha_e\nabla T) + \rho^{-1}\langle\mathbf{J}\rangle^2/\sigma, \quad (3)$$

where $\mathbf{v}$ is the velocity vector; p, the pressure; ρ, the density; $\nu_e = \nu_T + \nu$ is the effective viscosity (sum of turbulent and laminar viscosity) which is variable in time and position, $\langle\mathbf{f}\rangle$ is the locally time-averaged electromagnetic force; $\mathbf{g}$, the gravity vector; T, the temperature; $\alpha_e = \alpha_T + \alpha$ is the effective thermal diffusivity; C_p, the specific heat; C_p^*, the solid fraction modified specific heat function which accounts for latent heat effects (see [12] for details), and $\langle\mathbf{J}\rangle^2/\sigma$ is the Joule heat. The dynamic fluid flow problem is solved with the full set of the exact boundary conditions for a given time instant: at the liquid metal free surface the normal hydrodynamic stress is compensated by the surface tension only; the tangential stress is zero. In addition there is a kinematic condition, which states that the free surface locus is identical at all times to the fluid material particles. A no-slip condition is applied to the velocity at solid walls where there is contact at any given moment. The free surface contact position moves in accordance with force balance and the kinematic conditions. The temperature boundary conditions are expressed by the thermal flux (heat losses) to the surroundings: the radiation and the effective turbulent heat transfer at solid walls. The respective expressions are given in [12, 14, 15].

The fluid flow is turbulent, and the 2-equation k-ω time dependent turbulence model [13] is used to compute the efficient viscosity and turbulent heat transport. The temperature boundary conditions depend on the local effective thermal diffusion coefficient α_e at the wall and at the free surface, which is proportional to the effective turbulent viscosity ν_e determined from the numerical k-ω turbulence model. The appropriate k-ω model is the low Re number version which resolves the flow from laminar to developed turbulent states, and therefore is considered suitable both for the flow within the slow mushy zones and the bulk of the fully molten liquid metal at the final mixing stages. In the present work we apply the k-ω model within the pseudo-spectral framework [12, 14]. The computation follows in detail the time development of the turbulent characteristics determined by the coupled non-linear transport equations accounting for a continuous generation and destruction of the turbulent energy.

The pseudo-spectral spatial representation is used for the Navier-Stokes and the heat transfer Equations 1–3, and also for the k-ω model equations. In this approach the equations are satisfied exactly at the grid nodes, leading to a fully populated matrix solution. It is therefore possible to obtain a numerically well resolved problem on a rather coarse spatial mesh compared to the FV or FE methods. In addition, the solution is implicit in time, allowing for relatively large time steps coupled with iterative linearization of the non-linear terms in the equations. It is then possible to achieve a good turnaround time (less than 24 h on a Pentium III) for each full simulation [12]. The electromagnetic force distribution is highly sensitive to the shape of the liquid metal free surface and the material properties change with temperature. For this reason, the electromagnetic field is recalculated at each time step. The computational procedure for the electromagnetics is implemented on the same grid as the fluid dynamic equations. A Chebyshev polynomial Gauss-Lobatto radial distribution compresses the grid at the free surface ensuring a high degree of resolution within the surface boundary layer.

The electromagnetic force $\mathbf{f}$ is computed using a previously validated [12] integral equation algorithm. In cases where a combination of high frequency AC and DC magnetic fields has been used, we need further to obtain the time average of the force over the field oscillation period, which is of a very small time scale 10^{-3}–10^{-4} s. The electric current in the axisymmetric case is given by Ohm's law for a moving medium:

$$\mathbf{J} = \sigma(-\partial_t\mathbf{A} + \mathbf{v}\times\mathbf{B}) = \mathbf{J}_{AC} + \mathbf{J}_v, \quad (4)$$

where σ is the electrical conductivity, $\mathbf{A}$—the vector potential related to the magnetic field $\mathbf{B}$. The part of the

current $\mathbf{J}_{AC}$ is induced in the conducting medium in the assumption of the absence of velocity. It is computed according to the mutual inductance algorithm with elliptic integrals described in detail previously [12] and tested against analytical solutions and experimental measurements [14]. The same elliptic integral representation can be used to represent the DC magnetic field created by an additional external coil. The solution in the liquid volume depends on its free surface shape and needs to be recomputed when the shape changes. The resulting electromagnetic force $\mathbf{f}$, time-averaged over the AC period, similarly to (4) can be decomposed in two parts:

$$\mathbf{f} = \mathbf{f}_{AC} + \mathbf{f}_{v}, \tag{5}$$

where the second, fluid velocity dependent part of the force $\mathbf{f}_{v}$ in the axisymmetric and low magnetic Reynolds number case has the following components in spherical co-ordinates (R, θ, φ):

$$\begin{aligned} f_{vR} &= \sigma\left(-u\left\langle B_{\theta}^{2}\right\rangle - v\langle B_{R} B_{\theta}\rangle\right) \\ f_{v\theta} &= \sigma\left(u\langle B_{R} B_{\theta}\rangle - v\left\langle B_{R}^{2}\right\rangle\right), \end{aligned} \tag{6}$$

where the notation $\langle\cdot\rangle$ denotes time averaging over the AC period. The magnetic field components in the expressions (6) include AC and DC parts, both of which have a time average contribution to the force. It is of interest to note that, even if there is only an AC field, there is, in principle, an average $\mathbf{f}_{v}$ contribution to the interaction with the velocity field.

3. Modelling results: Validation and ISM modifications

The experimental part of the research programme was carried out at the University of Birmingham IRC using a 350 kW Consarc cold crucible furnace for melting various metallic alloys. The technical details, methodology and results were reported elsewhere [4, 15]. Melts were carried out in vacuum or in an argon atmosphere. The best results from the validation point of view were obtained in argon and for metals of lower melting temperatures like aluminium when a clear view of the melt surface can be maintained during the whole melting cycle and thermocouples can be used safely for temperature measurements in the melt. For all comparisons made, a good correspondence to the numerical results was obtained as reported in [4]. Here we will concentrate on the TiAl alloy melting cases and on those cases dealing with some modifications to the furnace parameters. Fig. 1 demonstrates a typical simulation result for the melting of a TiAl ingot, presented in a perspective view (this viewpoint corresponds to that obtained using a video camera attached to a furnace window [4]). The dome shape depicted is characteristic of all the melts.

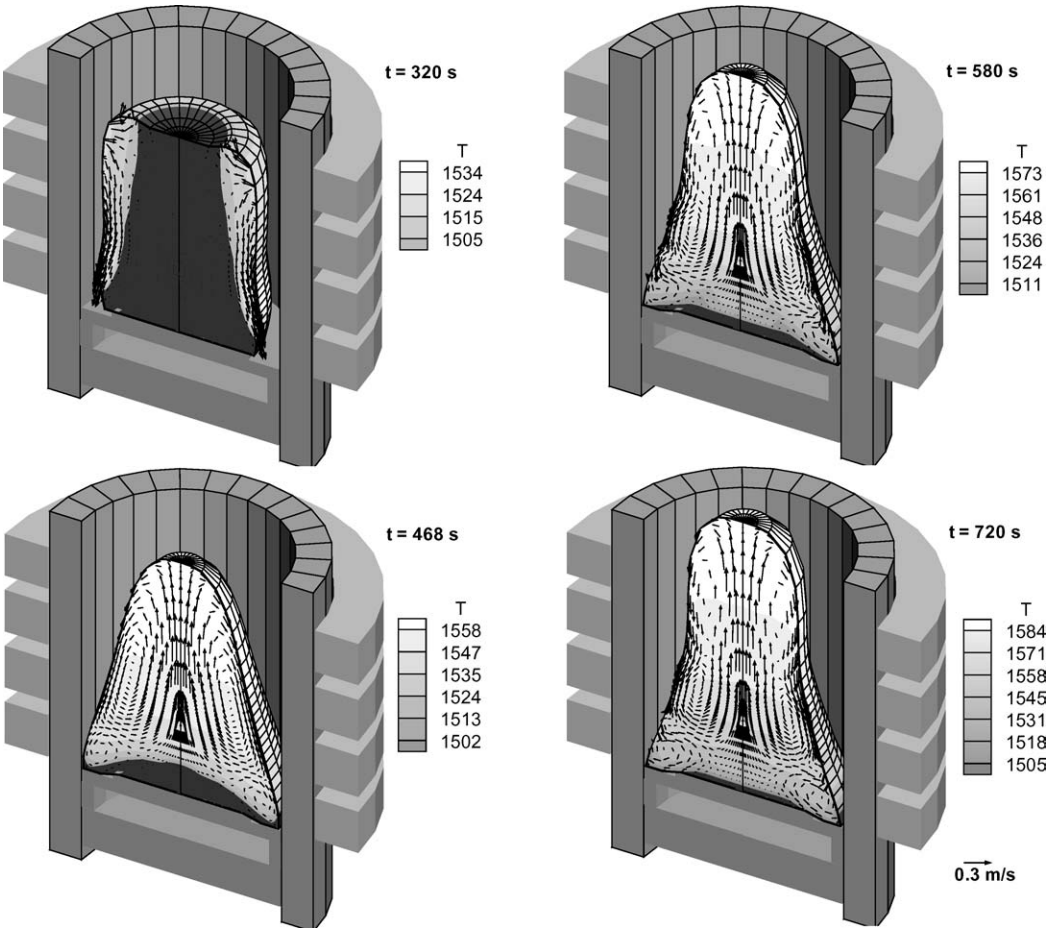

Figure 1 Views from the numerically simulated melting process of TiAl in the Birmingham IRC ISM furnace: ($t = 320$ s, $I = 4400$ A) first signs of melting appear at the cylindrical ingot edge, ($t = 468$ s, $I = 5600$ A) thick layer of solid metal left at bottom, ($t = 580$ s, $I = 6200$ A) the current increase in the coil leads to the superheat and deformation increase, ($t = 720$ s, $I = 6700$ A) melting completed with only a thin protective skull layer left at the bottom.

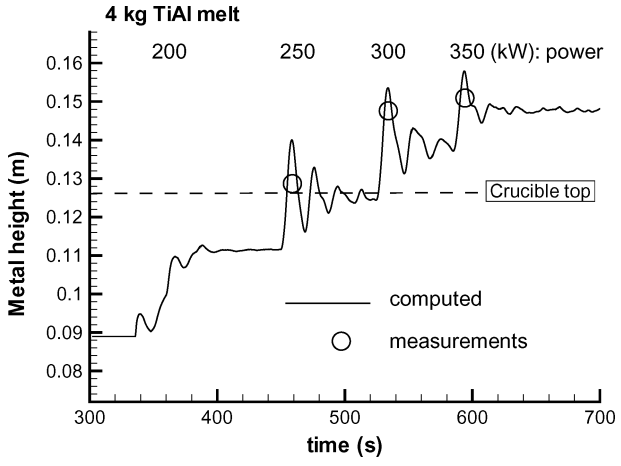

Figure 2 The computed liquid metal (TiAl alloy) top surface position change during the supplied AC field power increase and the three available instantaneous measurements [4].

Some information about the liquid metal dome height was directly obtained by measuring the level at which a wire immersed in the melt was completely melted away [4]. Fig. 2 shows this result for the TiAl melts where the molten wire end level relative to the crucible top is recorded. From the numerical simulation results we can see that the dome actually oscillates during the melt, with a damped oscillation accompanying each step change in power input. The dome height increases as the current magnitude increases. The free surface oscillations were observed in the experiments as well although their frequency was not recorded. The intensity (amplitude) of the oscillations depends on a variety of factors, like the relative value of the current increase step, the magnetically confined metal column shape prior to the current increase, and the turbulent effective viscosity damping response, which depends on the flow prehistory. Typically the oscillation dies away when the current is kept constant. However for some cases the oscillation can persist for a long time. If the current is abruptly increased in magnitude by a large value, metal can be physically ejected out of the crucible. In the numerical simulation this phenomenon is detected as a continuous increase in the metal column height until numerical instability sets in.

In the experiments the initial charge is usually a cylindrical ingot. The current in the induction coil is increased gradually in steps, and the calibrated curve relating the current magnitude to the power measured at the supply source is used as input to the computations [4]. The simulation shows the following sequence of events. Once melting starts, the temperature is highest in the surface film zone and the heat slowly penetrates the rather thick cylindrical charge in the radial direction (Fig. 1, $t = 320$ s). The flow is directed mainly downwards under the action of gravity, whilst the electromagnetic forces confine and oppose the waving downward motion of the film. Shortly, the melt reaches and fills the bottom gap between the ingot and the crucible wall. After this initial stage, i.e., when the bottom is filled, the largest Joule heating concentration is shifted to the bottom part of the side skin layer since this is now closest to the source coil and to the induced electric currents in the segmented wall. Subsequently the melting front progresses slowly radially inwards. The heat transfer by conduction within the solid part is small compared to that governed by turbulent advection in the flow region, and the phase change from solid to liquid consumes significant energy. The electric current and therefore the Joule heating source are induced in the side skin-layer, whence the intense turbulent mixing distributes the heat. The water-cooled base takes away the heat efficiently when the bottom gap is filled (Fig. 1). No significant destruction of turbulence occurs at the free surface with the zero stress boundary condition.

The most important problem for the cold crucible melting technique remains the control of heat transfer to the water cooled walls and bottom. Heat lost in these two regions makes the process very inefficient and limits the achievable superheat in the molten metal before it is cast in a mould. Experiments and numerical simulations were carried out to obtain an understanding of the temperature changes during the melting process and the heat transfer losses to the walls. In aluminium melts a thermocouple was used to record the temperature during the melting stages [4]. The heat losses from both the side wall fingers and the bottom of the crucible were measured using the temperature difference ΔT between the outlet and inlet coolant in the respective branches. Knowing the flow rate V, the coolant density ρ and the specific heat C_{p}, it was possible to obtain estimates for the heat flux Q (W) to the coolant at any given time moment during the melting cycle by using the equation:

$$Q = \rho \cdot C_p \cdot V \cdot \Delta T. \tag{7}$$

The results for an aluminium melt were published in [4, 15] together with the modelling validation. The heat losses to the crucible walls, composed of (a) Joule heating directly released within the wall V_{w} material and (b) the heat fluxes from the melt, can be computed numerically from the following expression:

$$Q_{\mathrm{W}} = \oint \rho C_{\mathrm{p}} \alpha_{\mathrm{e}} \nabla T \cdot \mathbf{n}\, \mathrm{d}S_{\mathrm{n}} + \int \langle \mathbf{J}^2 \rangle / \sigma \, \mathrm{d}V_{\mathrm{w}}. \tag{8}$$

The heat loss is governed by turbulence because of the very high value of the turbulent thermal diffusion coefficient α_e compared to molecular conductivity. A thermal balance is achieved soon after the metal is fully molten: the total Joule heating input to the liquid metal equals the total surface heat loss. At this stage the melt temperature reaches a plateau. With the same electrical power input there is no further increase in the melt temperature (Fig. 3a). Even an increase in the supplied power ($t = 540$ s in Fig. 3a) gives very little increase in the liquid metal temperature, which again stays at new slightly higher plateau level. A very similar result is obtained also when melting TiAl and other materials, therefore a modification to the current melting procedure is necessary in order to increase the melt superheat.

The numerical simulation of the ISM process facilitates a deeper understanding of the reasons for this energy loss and helps to find new ways to improve

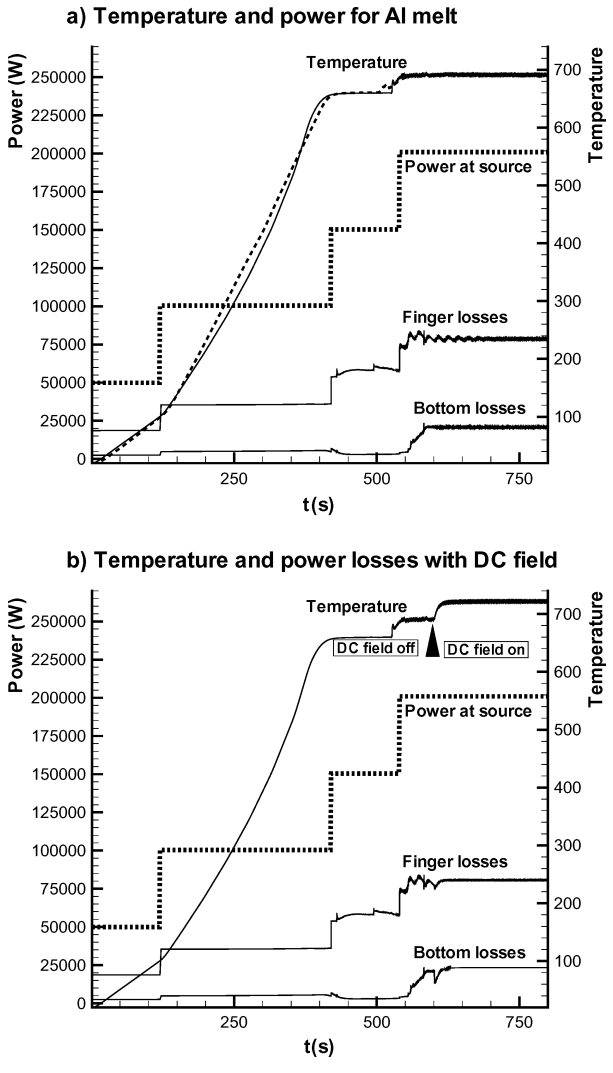

Figure 3 (a) The measured (dashed line) [4] and the computed (solid line) temperature and power losses for aluminium melt during the supplied AC field power increase (step-like dotted line 'Power at source'). (b) The marked increase of the temperature occurs at $t = 600$ s, when the additional DC current of 10 kA is switched on in the bottom coil.

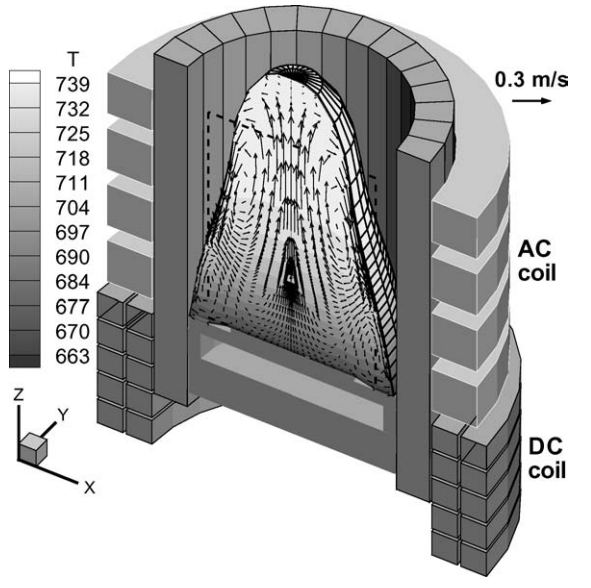

Figure 4 The velocity and temperature field in the aluminium melt at $t = 600$ s, when the DC current of 10 kA is switched on in the bottom coil.

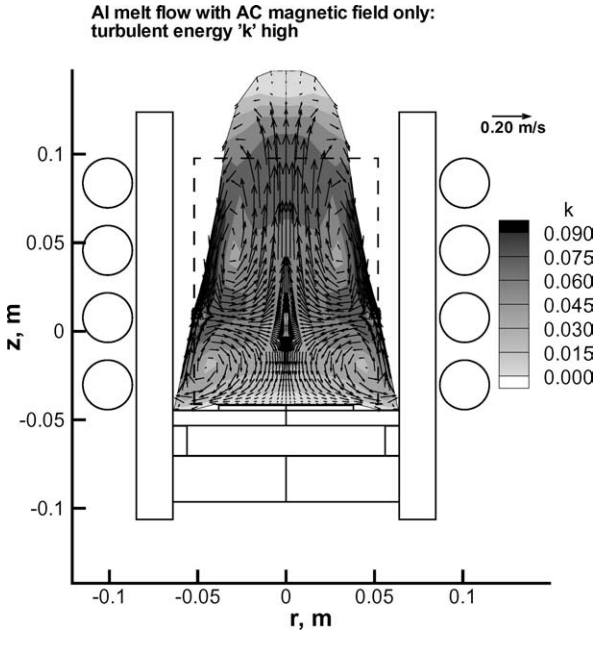

Figure 5 The velocity and turbulence kinetic energy distributions in the aluminium melt at $t = 600$ s without the DC current in the bottom coil.

efficiency. One of the methods devised to increase the melt superheat is illustrated in the Fig. 4. An additional coil carrying DC current is placed towards the bottom part of the crucible. The DC magnetic field created by this current easily penetrates the melt volume, the field intensity being the highest at the bottom. The resulting electromagnetic force from the induced AC current and the DC magnetic field is purely oscillatory, with no mean contribution. However, by introducing a relatively high DC magnetic field one directly affects the moving electrically conducting liquid owing to Equation 6; generally this leads to damping of the flow intensity and reduction of the turbulence level within the melt. The effect can be instructively demonstrated (see Fig. 3b) by the computed temperature behaviour, when a DC current of 10 kA magnitude is abruptly switched on at 600 s. The temperature jumps by about 40 degrees from the previous plateau, while maintaining the previous AC power input. A deeper insight into this phenomenon can be obtained from the comparison of Figs 5 and 6. The former shows the fluid velocities and the turbulent kinetic energy distribution in a vertical cross-section of the melt just before the DC field is switched on: the velocities are high, the turbulence level also. After the DC field is switched on, it takes just about 3 s to damp the velocity field and its gradients at the bottom where the DC magnetic field is the highest (Fig. 6). The overall turbulence level is reduced, and especially since this effect is felt in the bottom part, the turbulent thermal loss is significantly reduced.

Without this device, a similar increase of temperature would be equivalent to an additional 100–150 kW of AC power input. In practice however this would be impossible to realise, since melt deformation would then expel the metal from the furnace. In contrast, the DC field addition damps the fluid velocities and the interface instabilities also. This approach looks very promising for future ISM designs.

The dynamic modelling of the ISM melting can suggest many other ways of increasing energy efficiency. In

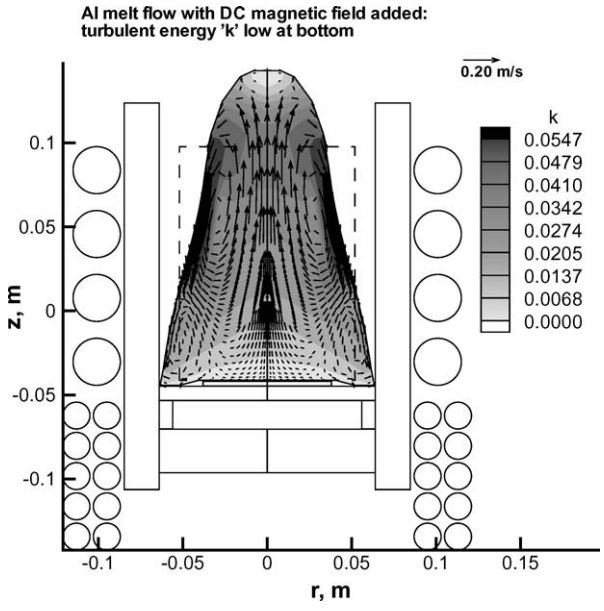

Figure 6 The velocity and turbulence kinetic energy in the aluminium melt at $t = 603$ s with the additional DC current of 10 kA in the bottom coil.

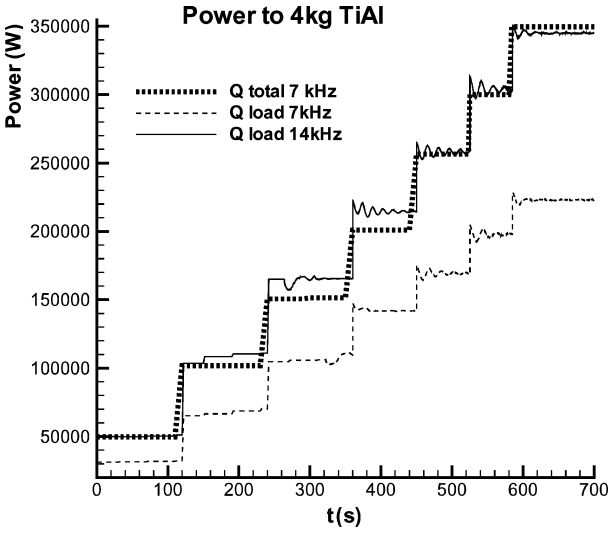

Figure 8 The calculated power (Joule heating) released in the furnace (the TiAl melt plus the copper crucible fingers and bottom) for two different AC frequencies during the same coil current step-like increase to the maximum of 6700 A corresponding to the experimental 'Power at source' for 7 kHz case.

TiAl melts it was not possible to measure the continuous long term temperature variation in the melt, due to the very limited life of the thermocouples at temperatures of 1500–1600°C. In this case only short time measurements were made using a Pt/Pt-Rh thermocouple protected with a Mo sheath [15]. The results for 4 kg of TiAl melting and the corresponding step increase in power are shown in Fig. 7 together with the equivalent continuous simulation result. Fig. 7 demonstrates also the temperatures for the simulated melts as a function of metal ingot charge weight. While keeping the input power at source the same for all charge weights (with the coil current calibration from the previously mentioned experiments), the resulting temperatures at the top part of the molten metal are significantly different. The reason is mostly related to the electrical efficiency of the coupled system; the higher "filling factor" leads to higher efficiency and as a result higher temperature. However, there is a limit to this filling factor increase, imposed by the ability to confine the melt with the given electromagnetic field so that contact with the water-cooled walls is prevented. For instance, the 6 kg charge reaches the limits for the particular crucible/coil combination.

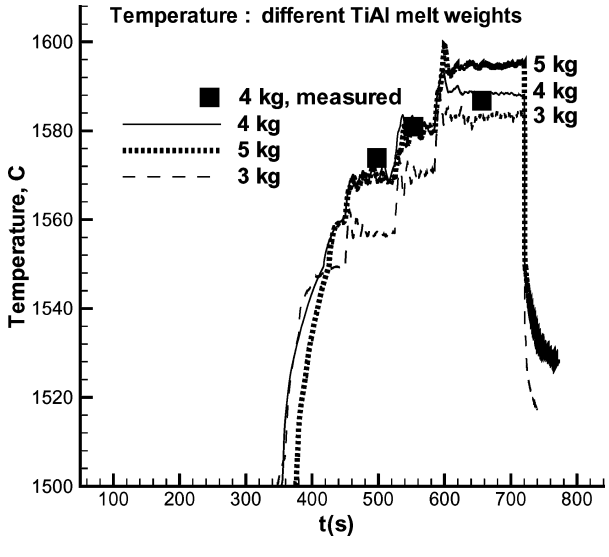

Figure 7 The numerically simulated TiAl melt temperatures for different charge weights. The limited measured temperature data [4] for the 4 kg load is shown as reference.

Another important design factor, concerns the role of AC current source frequency. This is quite a controversial subject for practical ISM applications where much of the practice is based on hearsay rather than a solid theoretical basis. In theory the power released within the inductively heated charge increases proportionally to the square root of AC frequency. However this is true for a given fixed external magnetic field intensity or, equivalently, when the current in the exciting coil is kept fixed. In practical large scale applications the power from the source would be the limiting parameter and, as a result, the current is adjusted to that. The higher frequencies generally mean increased losses in the power source itself and in the supplying cables. To gain some insight into the effect of frequency variations, one may consider first Fig. 8. In this figure the power (Joule heating) released within the TiAl charge melt and within copper crucible (fingers and base) at two different AC frequencies is computed (whilst keeping the supplied AC coil current magnitude increase the same as for the 7 kHz case above. It can be seen that even a relatively modest frequency of 14 kHz leads to high overall power dissipation in the crucible, which actually uses the full 350 kW level presumably supplied at the source for the whole system (load + losses in cables and power source). In fact, at 14 kHz the estimated total power, including the losses outside of the furnace, would be about 500–600 kW, a power level that could be best utilised at a lower frequency to achieve an even higher superheat.

The optimum frequency can be found through a systematic numerical study. As an example, Fig. 9

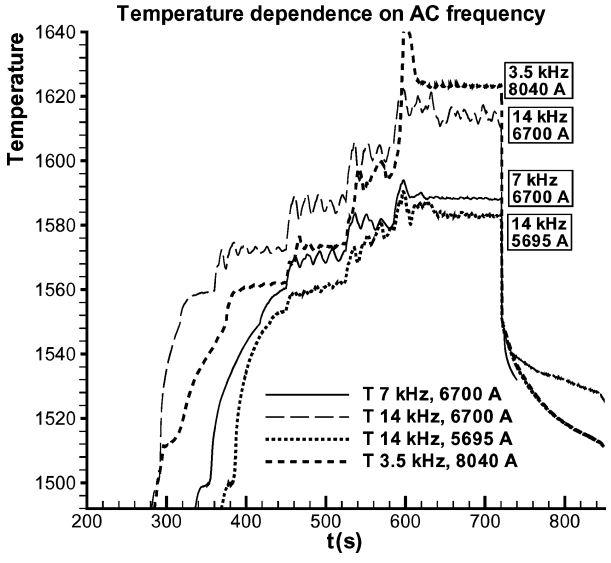

Figure 9 The calculated temperatures in the 4 kg TiAl melt for different AC coil frequencies. The reference case for 7 kHz and 6700 A maximum current corresponds to the experiment [4] represented on Fig. 7. The curve for 14 kHz and 5695 A maximum current is obtained when the power released in the metal + crucible is fixed equal to the reference 7 kHz case. Similarly, the case for 3.5 kHz and 8040 A corresponds to the same fixed power.

demonstrates this effect of frequency change on achievable temperature in the melt as predicted by the model. The 14 kHz case gives indeed significant temperature increase if the maximum current can be kept at the previously discussed level reaching a maximum of 6700 A (the same as for the test 7 kHz case). But we concluded in the previous discussion that this means a significantly higher power at the source, at 500–600 kW. If this power level is kept constant at 350 kW, then due to the various losses a maximum current of only 5695 A reaches the crucible and the resulting superheat within the melt is actually lower than for the 7 kHz case (Fig. 9). On the contrary, reducing the frequency, for instance, to 3.5 kHz and again fixing the power consumed by the furnace with the same metal charge, results in a significantly higher temperature within the melt (the maximum available current here is 8040 A). In the latter case the metal shape is highly distorted and stability would be a problem; a further adjustment of the frequency or the coil shape and position is needed to stabilise the situation while maintaining the high superheat. The consequences of these numerical experiments could be of high importance for practical applications.

4. Conclusions

A numerical model was presented of the full melting cycle in an ISM furnace. The model features the coupled effects of free surface, electromagnetic field and turbulent flow. The model was validated against direct measurements of melt shape, temperature and thermal loss on a commercial size ISM furnace. It was then applied as a design tool to evaluate the effect of various design and operational modifications on obtainable superheat. The simulations explain and quantify the factors contributing to thermal inefficiency and based on this understanding solutions have been proposed. Hence, the computations point to the advantages of the addition of an external DC field in damping turbulence and stabilising the melt shape. Other factors such as the coil shape, position, frequency choice and the load fill factor are shown to have an effect on efficiency and are therefore candidates for optimisation.

Acknowledgments

The financial support of the EPSRC in this research is gratefully acknowledged.

References

1. H. TADANO, K. KAINUMA, T. TAKE, T. SHINOKURA and S. HAYASHI, in Proceedings of the 3rd International Symposium on Electromagnetic Processing of Materials (ISIJ, Nagoya, Japan, 2000) p. 277.
2. M. VOGT, F. BERNIER, A. MUEHLBAUER, M. BLUM and G. JARCZYK, in Proceedings of the 3rd International Symposium on Electromagnetic Processing of Materials (ISIJ, Nagoya, Japan, 2000) p. 289.
3. P. GILLON, in Proceedings of the 3rd International Symposium on Electromagnetic Processing of Materials (ISIJ, Nagoya, Japan, 2000) p. 635.
4. R. A. HARDING, M. WICKINS, V. BOJAREVICS and K. PERICLEOUS, in "Modeling of Casting, Welding and Advanced Solidification Processes, **X**," edited by D. M. Stefanescu *et al.* (TMS, Warrendale, 2003) p. 741.
5. Y.-Q. SU, J.-J. GUO, G.-Z. LIU, J. JIA and H.-S. DING, *Mater. Sci. Techn.* **17** (2001) 1434.
6. T. TANAKA, K. KURITA and A. KURODA, Liquid Metal Flows ASME 1991, FED-Vol. 115, p. 49.
7. M. ENOKIZONO, T. TODAKA, I. MATSUMOTO and Y. WADA, *IEEE Magn.* **29**(6) (1993) 2968.
8. E. BAAKE, A. MUEHLBAUER, A. JAKOWITSCH and W. ANDREE, *Metall. Mater. Trans.* B **26B** (1995) 529.
9. P.-R. CHA, Y.-S. HWANG, Y.-J. OH, S. H. CHUNG and J.-K. YOON, *ISIJ Intern.* **9** (1996) 1157.
10. F. BERNIER, M. VOGT and A. MUEHLBAUER, in Proceedings of the 3rd International Symposium on Electromagnetic Processing of Materials, ISIJ, Nagoya, Japan, 2000, p. 283.
11. M. CROSS, C. BAILEY, K. PERICLEOUS, A. WILLIAMS, V. BOJAREVICS, N. CROFT and G. TAYLOR, *J. of Metals, JOM-e*, 2002 January: http://www.tms.org/pubs/journals/JOM/0201/Cross/Cross-0201.html
12. V. BOJAREVICS, K. PERICLEOUS and M. CROSS, *Metall. Mater. Trans.* B **31B** (2000) 179.
13. D. C. WILCOX, Turbulence Modelling for CFD, 2nd ed. (DCW Industries, California, 1998).
14. A. BOJAREVICS, V. BOJAREVICS, J. GELFGAT and K. PERICLEOUS, *Magnetohydrodynamics* **35**(3) (1999) 258.
15. V. BOJAREVICS, G. DJAMBAZOV, R. A. HARDING, K. PERICLEOUS and M. WICKINS, in Proceedings of the 5th Int. Conf. on Fundamental and Applied MHD 'PAMIR' (Ramatuelle, France, 2002) Vol. 2, p. 77.

Received 10 March
and accepted 21 June 2004